How to cite: *Angew. Chem. Int. Ed.* **2021**, *60*, 24257–24265
International Edition: doi.org/10.1002/anie.202110725
German Edition: doi.org/10.1002/ange.202110725

Nanofibers

General, Metal-free Synthesis of Carbon Nanofiber Assemblies from Plant Oils

Liyuan Zhang, Xinzhe Li, and Markus Antonietti**

Abstract: *We designed a metal-free synthesis of carbon nanofiber based on ketene chemistry using phosphorus pentoxide (P_2O_5) and vegetable oil. Based on the characterization of intermediates, P_2O_5-oil reaction yielded most possibly alkylketenes, which polymerized into poly(ketene) with abundant enol groups. The enol groups further reacted with P_2O_5, forcing the poly(ketene) to assemble into a nano-sized preassembly structure. Moderate heating transforms these structures into carbonaceaus nanofibers. This approach is applicable to other chemicals with similar structure to vegetable oil. The carbon nanofibers with P-O-C functionalization show relatively high graphitization degree and promising textural properties. The C-O-P environment accounts for 66 at% of the total P and creates a superior thermal stability. As a model application, a CDI system built of a carbon-nanofiber-based electrode countered by an activated carbon-based electrode exhibited exceptional performance.*

Introduction

Carbon nanomaterials exhibit many intriguing physical and chemical properties, which include electrical conductivity, chemical stability, high specific surface area, and many more.[1] Due to these features, carbon is applied in a broad range of applications, such as adsorption, energy storage, sensors, or catalysis.[2] Other than the 3D and 2D carbon species, 1-dimensional (1D) carbon nanomaterials possess an ultrahigh aspect ratio. 1D carbon nanostructures thereby have many interesting properties (e.g., mechanical stability while being flexible, or directed conductivity), which attracted extremely high attention world-wide.[3]

In that search, a variety of 1D carbon nanomaterials, such as carbon nanofibers, nanobelts, nanobranches, nanorods and nanotubes, have been reported.[4] Popular choices of bulk synthesis include chemical vapor deposition, template processes, but also molten salt technique.[5] Generally, to direct carbon growth in 1D direction, metals or metal compounds are indispensable. Despite of sometimes even high efficiency, these methods still suffer from impurities. For instance, metal catalysts could not be completely removed by acid etching;[2i] or metal chlorides evaporate and contaminate synthesis lines and outer environment.[6] Therefore, we felt tempted to develop a robust chemical synthesis of 1D carbon nanomaterials on the base of simple, regrowing educts without using metallic species. Up to the best of our knowledge, such synthetic processes have been not described.

The most traditional source of sustainable carbon is biomass, as done for instance for the synthesis of charcoal or activated carbons. As compared with the mostly used lignocellulosic biomass, vegetable oils are hardly used for carbonization, as they are mostly C–H bond based and not known to give high carbonization yields.[5d] The structure is composed of fatty acids esterified to glyceride (Scheme 1).[7] Vegetable oils are abundant, low-cost, and even after excessive kitchen use still applicable in carbonization reactions. A secondary use in the chemical synthesis of 1D carbon nanostructures thereby follows the concept of upcycling.

Herein, we used the special structure of vegetable oils to develop a metal-free chemical route to synthesize towards carbon nanofiber assemblies. We used the reaction of oils with P_2O_5 to create first an amphiphilic addition product, which self-organized towards nanoscopic cylindrical micelles. Thermal elimination of the alkyl tail not only generates a hydrocarbon side product which could be isolated on a larger scale, but also leaves the wanted 1D carbon nanostructures as rather pure products. Noticeably, the previous reports, which mainly relying on the dehydration effect of P_2O_5 to produce carbon dots, thin carbon nanostructures or other carbonaceous materials,[8] are obviously different from ours. As shown by diverse analytical characterization techniques, the carbon nanofibers are not only 1D, but are doped with abundant P-O-C groups within their structure, bringing high water wettability, polarity, and ion binding into the structure. Due to the high electronic conductivity and the high ionic character at the same time, these novel 1D carbon nanofibers could be favourably applied in diverse ionotronic applications, such as CDI to remove the NaCl from a model seawater.

Results and Discussion

The chemical synthesis started with mixing of P_2O_5 (10.0 g) and vegetable oils (10.0 mL) together at room

[*] Dr. L. Zhang, Prof. M. Antonietti
Max Planck Institute of Colloids and Interfaces
Am Mühlenberg 1, 14476 Potsdam (Germany)
E-mail: atomic_liyuan@yeah.net
office.cc@mpikg.mpg.de
Dr. X. Li
Department of Chemistry, National University of Singapore
3 Science Drive 3, Singapore 117543 (Singapore)

Supporting information and the ORCID identification number(s) for the author(s) of this article can be found under: https://doi.org/10.1002/anie.202110725.

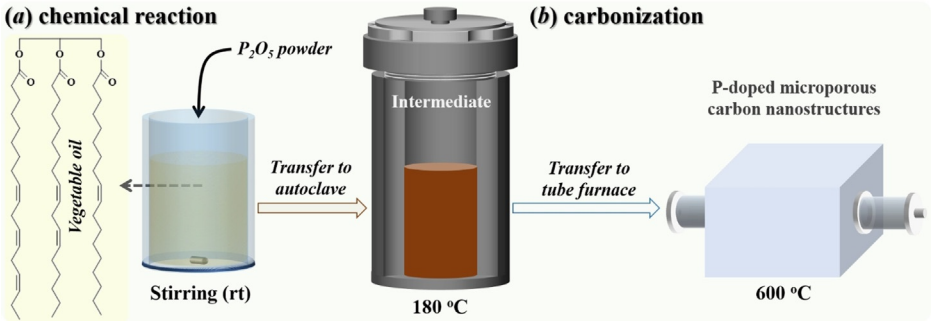

Scheme 1. Synthetic pathways of the P-O-C functionalized carbon nanofiber bundles: a) chemical reaction between P_2O_5 and vegetable oils[17] to form the intermediate and b) carbonization of the intermediate from the chemical reaction in step (a).

temperature by vigorous stirring to promote intense contact. Then, the mixture was transferred into an autoclave, which was held at 180 °C for 12 h. In this time, P_2O_5 integrates into the oils structure and promote intermediary self-assembly as described below. The as formed clear organic liquid generated during the reaction is not wasted, but a side-product composed of alkanes, alkenes, and thermal aromatization products in mixture similar to gasoline (Figure S1). The already dark brown intermediate is a fine sludge and oily phase, which was for simplicity directly carbonized in tube furnace at 600 °C to acquire the P-O-C functionalized carbon nanostructures. Here, at least a majority of alkyl tails fragments and leaves the sample. The process was also illustrated for better understanding in Scheme 1. The final materials are named by CNb-oil*y*, where *y* represented the ratio of P_2O_5 mass to oils volume. More detailed information is given in Materials-S1. Interestingly, final product contains P_2O_5 reformed after reaction, which promises a partial recovery of the P source as the most expensive part of the reaction. Another major part of P stays however incorporated into the carbon structure. As shown, the weighted out mass yield increases with the increase of P_2O_5 dosage. Specifically, the yield is 7.96 %, 18.50 %, and 32.99 % for CNb-oil*0.5*, CNb-oil*1* and CNb-oil*1.5*, respectively, pointing to an increasing P-O-C content. Noticeably, no oil residue can be found in the final product, as proved with FTIR characterization (Figure S2).

Scanning electron microscopy (SEM) was carried out to depict the morphology of the CNb-oil*1* (Figure 1). Basically, the carbon materials show a family of fibrous morphologies, namely shorter fibers aligning to spindles (Figure 1 a), bundles (Figure 1 c) and "haystacks" (Figure 1 e). From the higher magnification images, it could be clearly confirmed that these three assemblies are all composed of carbon nanofibers. Moreover, the nanofibers are very uniform in size and shape. The carbon nanofibers tend to be parallel to each other (Figure 1 b, d and f). The cross-section image of CNb-oil*1* further confirmed the nanofibers alignment (Figure 1 g and 1h). When the relative dosage of P_2O_5 was increased to 15.0 g without changing the oil volume (CNb-oil*1.5*), nearly only the nanofiber-based spindles could be found with the well alignment of the uniform fibers (Figure S3). However, decreasing the relative dosage of P_2O_5 to 5.0 g (CNb-oil*0.5*), a major part of assemblies becomes irregular, but there is still a small number of nanofiber-based spindles (Figure S4). Basically, carbon nanofibers are the sole building blocks from the carbonization of P_2O_5-oil intermediate, which assembled into specific superstructure.

Transmission electron microscope (TEM) was conducted to investigate the microstructure of carbon nanofibers. As seen in Figure 2 a, the fibers-aligned assemblies can be vividly confirmed in the low magnification image. Moreover, isolated nanofibers could be found in high magnification TEM images (Figure 2 b), which displays a partially hollow architecture. This could be further supported by AFM characterizations, as for instance shown in Figure S5. The diameter range of single nanofiber based on TEM and AFM is 22–41 nm and 37–60 nm, respectively. Moreover, from the AFM result, the wall thickness of the nanotube is between 1.01–1.64 nm. From the TEM image in Figure 2 c, the CNb-oil*1* at least appears locally disordered, i.e., as amorphous carbon. Energy dispersive spectroscopy (EDS) mapping images of the CNb-oil*1* were conducted to examine the element distribution. As seen in Figure 2 d, the elements C, P, and O are uniformly dispersed among the carbon nanofibers, marked by red, green, and yellow colors, respectively. The morphology of the other two samples is similar to that of CNb-oil*1*, as judged by TEM (Figure S6).

To reveal the possible mechanism in more detail, the intermediates and vegetable oils were characterized with FTIR technique (Figure 3). Different samples were obtained by capturing the intermediates at different temperatures, i.e., 80 °C, 180 °C, 350 °C, 400 °C, 425 °C and 450 °C (named intermediate-xC, where *x* is temperature value). Based on the FTIR spectra in Figure 3 a, the structural change of the vegetable oils before and after the P_2O_5-reaction is easily followed. In typical, the ester groups in oils disappear after the reaction at temperatures exceeding 350 °C, and correspondingly, C-O-P and > C=C < emerge. For the intermediate-80C, there is still P-O-P in the structure but > C=C < still has not formed. The peak broadens when temperature is higher than 180 °C, and new broad peaks in the range of 1550–2200 cm^{-1} form.

In fact, the cleavage of P-O-P in P_2O_5 and C-O in oils triggers the formation of the C-O-P group, just as the compound ***i*** in Figure 3 c, consuming at the same time the C-O. Generally, intermediates similar to compound ***i*** are known to decompose into ketene-based structures,[9] and the ketene here is the well-known fatty acid ketene with a long

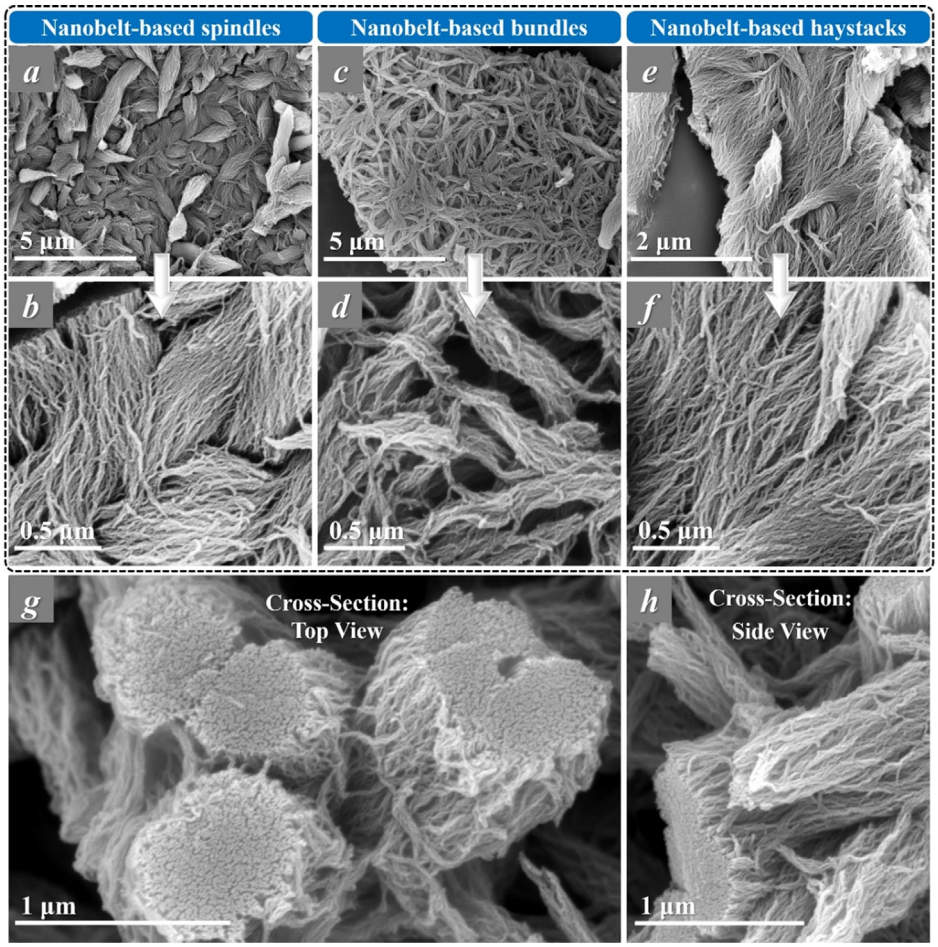

Figure 1. SEM characterizations of the CNb-oil*1* with three typical nanofiber-based assemblies: a),c),d) low magnification images; b),d),f) high magnification images. SEM images of the cross-section of CNb-oil1: g) top view and h) side view.

aliphatic tail, as it is used in paper hydrophobization. Moreover, as revealed by Staudinger,[10] Olah[11] and Wudl,[12] the ketene can readily polymerize into the so-called poly(ketenes) with abundant enol units (compound ***ii***), due to the high reactivity of ketene. Actually, the four broad peaks between 1550 and 2200 cm^{-1} can be assigned to the though-conjugated ketone structure in poly(ketene) (frame in Figure 3a).[1,12] This result can be confirmed with the ^{1}H-NMR characterization. As shown in Figure 3b, the new chemical shifts between 2.5–3.0 ppm can be found, which is caused by the ketone structures (R−CH−C=) in poly(ketene).[13] On the other hand, the hydroxyl groups are very easy to react with the remaining moiety of P_2O_5. Based on this process, compound ***ii*** would transform into the compound ***iii*** (Figure 3c).

In compound ***iii***, the long aliphatic chains are the hydrophobic tails, and the center C-O-P units are the hydrophilic cores, which together exhibits an amphiphilic property. In this context, it is reasonable to postulate that such molecules would spontaneously self-assemble into specific regular nanostructures. Here combining the morphology characterizations (Figure 1, Figure 2 and Figure S5) with the structural results, we hypothesized that the polymers formed assemble in an intermediary state to amorphous tube vesicles (Figure 3c and d). In the carbonization process, such a fictive compound would evolve into the observed belt-like nanofibers with partial still open hollow structure within them.

To further understand the applicability range of the method developed in this research, three control experiments were designed by using pure chemicals. Other synthetic process is completely identical to the case using vegetable oils. In the first control experiment, vegetable oils were replaced with the diethyl hexanedioate that has similar chemical features to the oils (e.g., ester group connected with aliphatic tail). As shown in Figure S8, it is interesting to find that the carbon materials possess similar morphology to the CNb-oil series. In the second control experiment, the carbon source becomes the 1,2-tetradecylene oxide that has a long aliphatic tail, but the ester group was changed to epoxy group. The carbon materials obtained are mainly composed of the 3D nanoparticles (Figure S9). No 1D carbon nanostructures could be acquired even in the presence of long aliphatic tail. In general, the epoxy-P_2O_5 reaction pathway is completely different from the P_2O_5-ester reaction, which actually would produce 3D cross-linked structure (Figure S7).[14] In this circumstance, the long aliphatic tails have no choice but could only distribute randomly in the 3D space, which leads to the formation of 3D carbon nanostructures. In a further

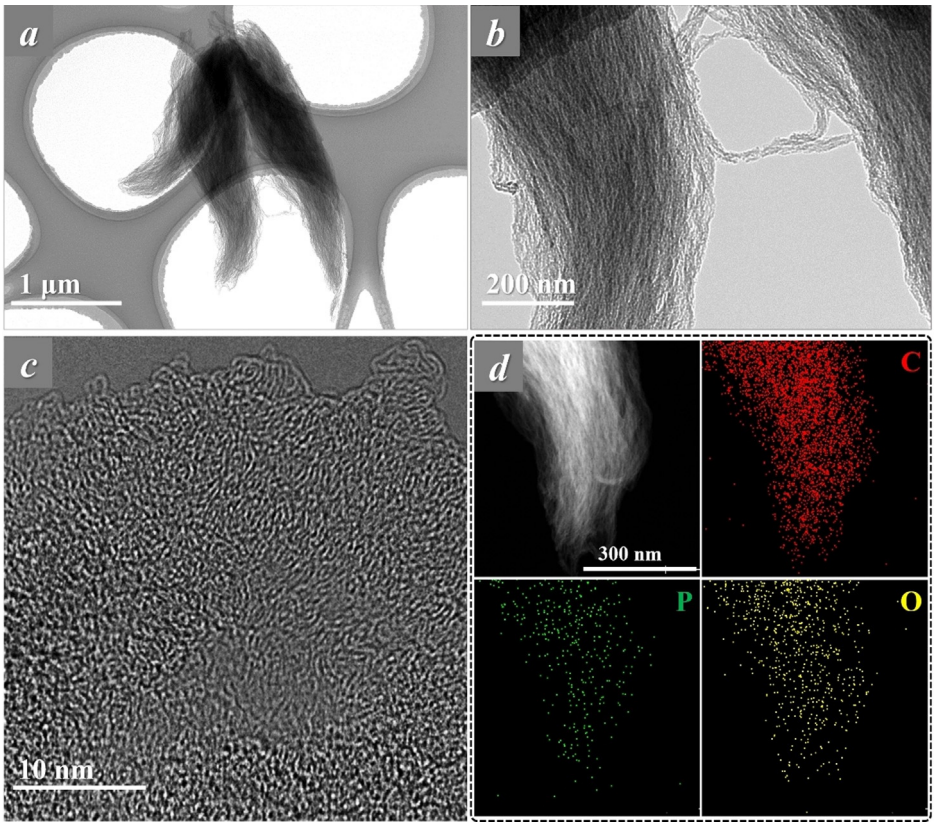

Figure 2. TEM characterizations of the CNb-oil*1*: a),b) microstructural morphology, c) high-resolution image and d) elemental mapping with C, P, and O.

control experiment, polyethylene glycol was used as carbon source to interact with P_2O_5. The reaction between ether group and P_2O_5 is similar to the epoxy-P_2O_5 interaction, but there is no long aliphatic tail in this chemical. Here only a hard and irregular macroscopic carbon block was obtained, which exhibited irregular microstructures (Figure S10). These control experiments as well as the main experiments together demonstrate that the in situ formation of intermediates with well-organized hydrophilic core and hydrophobic tail plays dominated role in the formation of uniform 1D carbon nanostructures. This could be an important guideline for the further design of the 1D carbon nanomaterials based on metal-free protocol. Based on these results, we conclude that carbon nanofibers could be synthesized from natural plant oils in general.

The structure of the left-over carbon can be characterized by a variety of local analytical techniques. XPS is a tool characterizing not only the amount of the elements, but also their mutual binding probability. As seen in Figure 4a, the elemental overview teaches us that the prevailing species is indeed C, with significant content of O and a distinct, but smaller amount of P. This already indicates that the vast majority of P is leaving in the synthesis at the end as P_2O_5 or phosphoric acid, i.e., it is mostly a catalyst and dehydration agent. This can be further proved with the elemental analysis (Table S1) that the C accounted for 73.3 at% in CNb-oil*1*. For the other two samples, the C content is also slightly higher than 70 at% (Table S1). Correspondingly, the high resolution spectrum for the C1s region (Figure 4b) is predominantly described as a C=C bonded structure. Noticeably, the C-O at 285.33 eV involved the C-O-C and C-O-P. This strongly demonstrates the P doping in the carbon nanofibers. A majority of the nanostructures seems to be surface terminated with C–x bonds. According to the high resolution O1s spectrum (Figure 4c) and P 2p spectrum (Figure 4d), the C-P bonds and C-O-P bonds are formed in the 1D carbon nanofibers. In typical, the C-O-P and C-P accounted for 66.22 at% and 39.78 at%, respectively, in the total P species. The formation of C-P should originate from the C-O-P in the intermediate as illustrated in Figure 3. Interestingly, the variation of the P_2O_5 dosage in the synthesis of carbon nanofibers could change the relative atomic percentage of the P components (Figure S11). Based on the survey spectra, the increased P_2O_5 dosage increased the relative content of P species. Moreover, the relative content of C-P to C-O-P dropped with the increase of P_2O_5 dosage, according to the P2p spectra.

The textural properties of the CNb-oil series were investigated by gas adsorption-desorption isotherms. Figure 4e presents the N_2 adsorption-desorption isotherm of the three materials. As shown, the steep increase of N_2 adsorption in the P/P_0 range of 0–0.1 and the loop in 0.4–1.0 indicated the hierarchical micro-meso porosity of the carbon nanofibers. Typically, the CNb-oil*1* exhibited the highest specific surface area among the samples, which reached to 780.9 $m^2 g^{-1}$. As given in Figure 4f, the pore size mainly distributed around

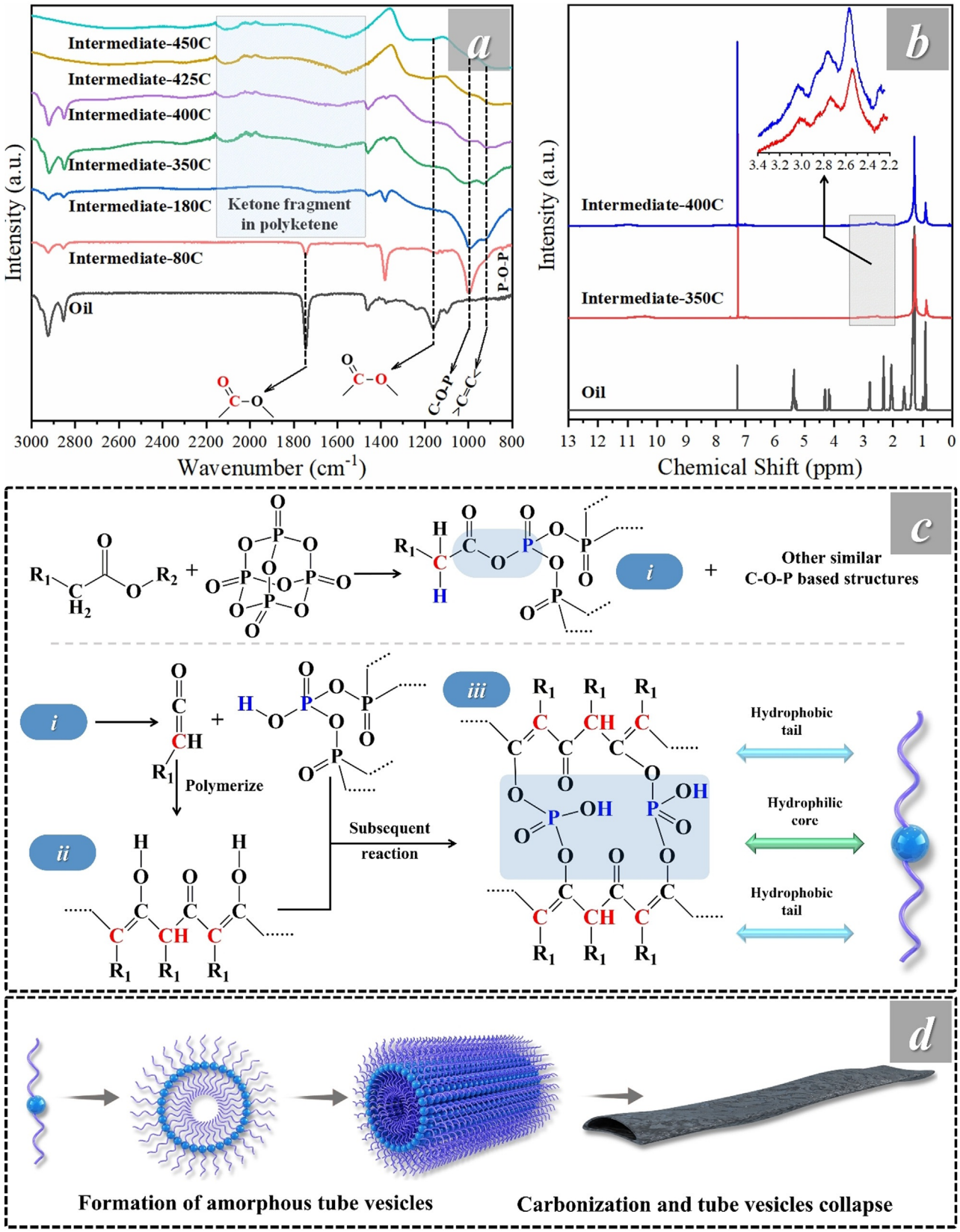

Figure 3. a) FTIR and b) ^{1}H-NMR characterizations of the intermediates. c) Possible reaction between P2O5 and vegetable oils to form the intermediates. d) Simplified model for the morphology evolution in the carbonization process of intermediates. Note: the intermediate is synthesized using the identical recipe as CNb-oil1."

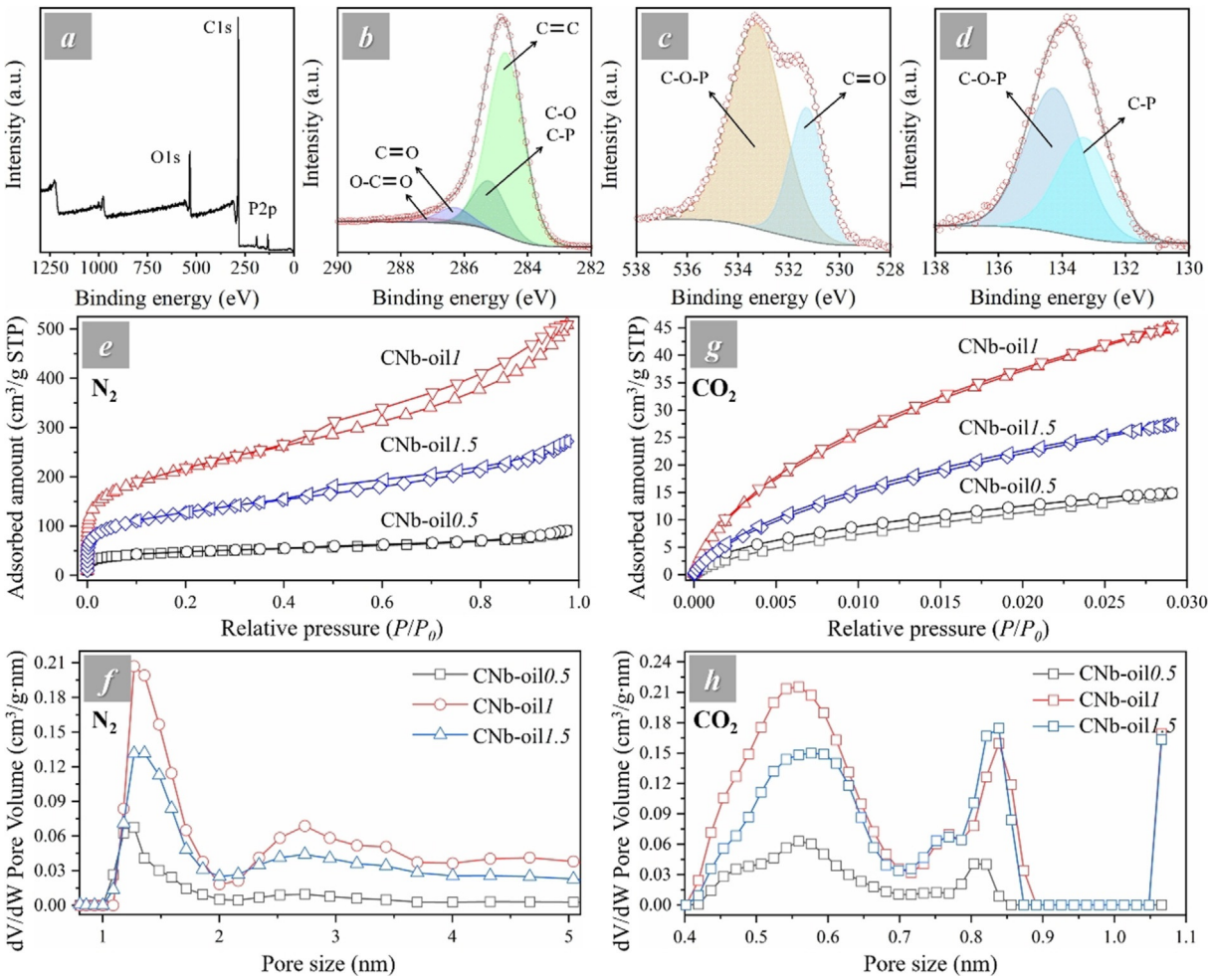

Figure 4. XPS spectra of CNb-oil*1*: a) survey spectrum, b) C1s spectrum, c) P2p spectrum, and d) O1s spectrum. e) N_2 adsorption–desorption isotherms, and f) pore size distribution of CNb-oil series.

2.73 nm and 1.27 nm. Combining the porosity with the 1D feature, the carbon nanofibers should possess additional benefits, as high mass transfer. Moreover, CO_2 adsorption-desorption isotherms (P/P_0 range: 0–0.03, Figure 4g) were taken to investigate potential ultramicropores of the CNb-oil series.[15] Figure 4h provides the pore size distribution of the three materials based on CO_2 isotherm, showing abundant ultramicropores in the CNb-oil series, centered around 0.56 nm and 0.84 nm. The texture properties are also summarized in Table S1. In particular, the pore volume of micropores only of CNb-oil*1* reaches values as high as 0.688 $cm^3 g^{-1}$.

Figure S12 gives the XRD patterns of the carbon nanofibers. There is a broad peak in ca. 26° and no other obvious diffraction peaks could be observed. This sufficiently indicates the amorphous nature of the carbonaceous products. In Raman spectra (Figure S13), the CNb-oil series displayed two sharp peaks at 1335 cm^{-1} and 1596 cm^{-1}, which could be due to the D peak and G peak, respectively. The I_G/I_D represented the graphitization degree,[16] and the I_G/I_D increased with the decrease of P_2O_5 dosage. Noticeably, the I_G/I_D can still reach 1.35 for CNb-oil*1.5*, which indicates a relatively good graphitization of the CNb-oil series. This is necessary for a high conductivity of the carbon nanofibers. Zeta potential of the carbon nanofibers was measured to understand their surface properties (Figure S14). As shown, the zeta potential of all materials is negative in a broad pH range from 1 to 11. Moreover, the zeta potential is even less than −30 mV when pH is higher than 5. The negative zeta potential is attributed to the many C-O-P chemical units in the samples. This combination of high electric conductivity with high ionic character might endow the materials with interesting "ionotronic" multifunctionality, which is potentially useful in many important applications. Additionally, the thermal stability of the carbon nanofibers (CNb-oil*1*) was investigated in comparison with single-walled carbon nanotubes (Figure S15). The CNb-oil*1* exhibits better thermal stability than carbon nanotubes, which we again ascribe to the C-O-P functionalization.

To evaluate the application potential, a capacitive deionization experiment (CDI) with electrodes built from carbon nanofibers was conducted. As illustrated in Figure 5a, CDI is composed of two electrodes, which deionizes brackish water by applying an electric potential between them. Prior to the performance evaluation, the electrochemical characterizations of CNb-oil series based on three-electrode system were

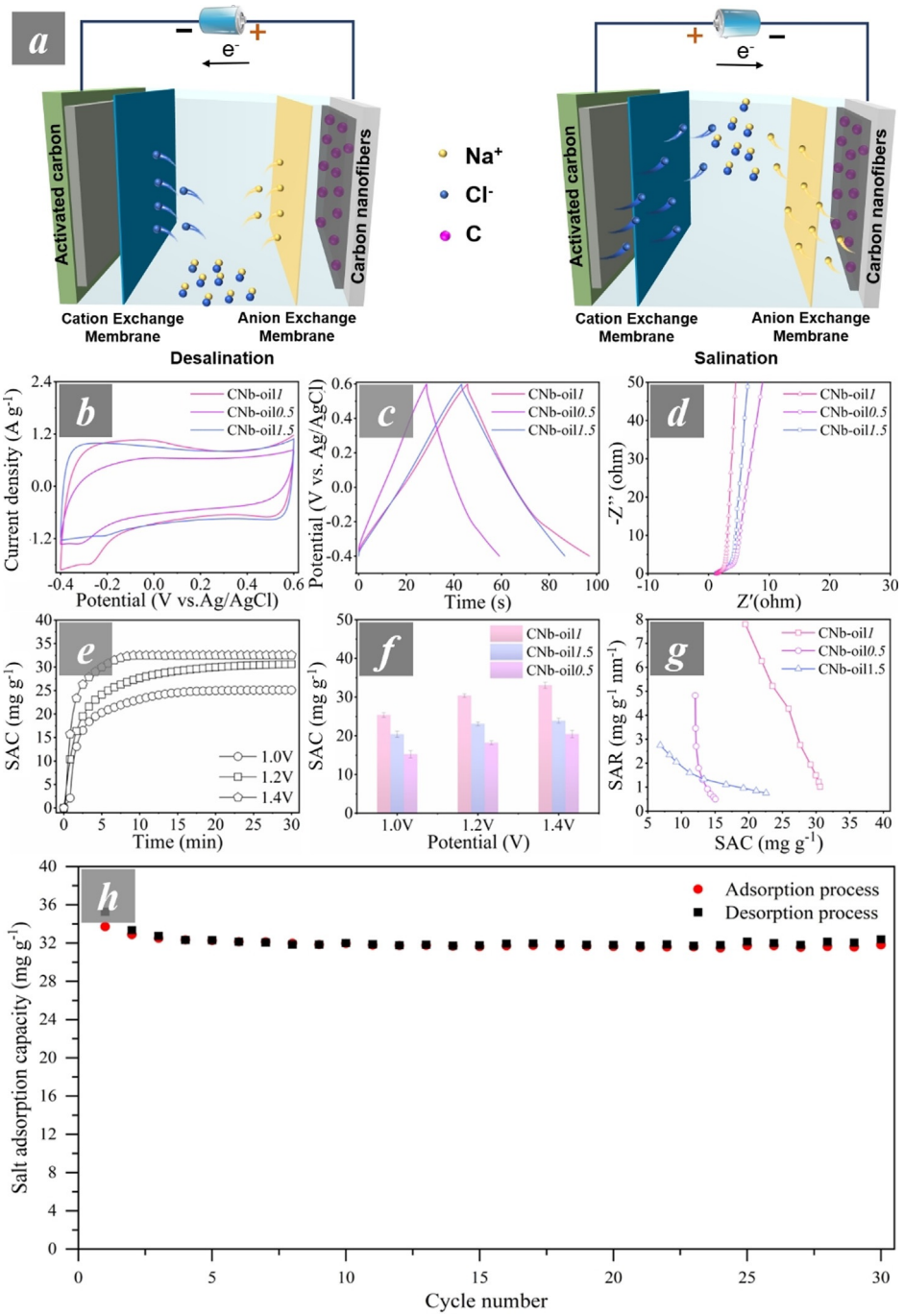

Figure 5. a) Illustration of the working principle of capacitive deionization (CDI). Electrochemical performance of the CNb-oil series: b) CV curves of different electrodes at a scan rate of 10 mV s^{-1}, c) Galvanostatic charge-discharge curves, d) the Nyquist plots. CDI performance evaluation of the CNb-oil series-based electrodes with NaCl concentration of 500 mg L-1: e) electrosorption capacity with time, f) SAC in different potential, g) SAR-SAC Ragone plot, and h) long-term cycling performance.

examined by cyclic voltammetry (CV) and galvanostatic charge-discharge (GCD) measurements in a 1.0 M NaCl solution following three-electrode conditions. The quasi-rectangular shape of CV curves of the CNb-oil series (Figure 5a) indicates the dominant behavior of electric double-layer capacitance. Correspondingly, as shown in Figure 5b, the GCD result of CNb-oil*1* presents a nearly symmetric triangular shape with the longest discharge time, demonstrating a superior capacitive performance. Figure 5c gives the EIS measurement result, from which the CNb-oil*1* possesses the lowest resistance.

The CDI performance of the CNb-oil series was evaluated in 500 mg L^{-1} of NaCl solution to understand their practical application potential. The CNb-oil series-based electrode is for adsorbing the Na^+ while the activated carbon-based electrode is for adsorbing the Cl^-. The specific adsorption

capacity (SAC) of the CNb-oil*1* with time in Figure 5d shows that the adsorption process is fast, which costs ca. 15 min at most to reach equilibrium. Typically, the equilibrium time would further shorten by increasing the applied voltage. Figure 5e shows the SAC of the CNb-oil series as a function of the applied voltage. As shown, the SAC increases with the increase of the applied voltage. Moreover, the CNb-oil*1* owns the highest SAC among the three samples, which is ca. 30 $mg\,g^{-1}$ at 1.2 V. Figure 5f further provides the CDI Ragone plots of the CNb-oil series-based electrodes, and the CNb-oil*1*-based electrode displays the highest SAC and specific adsorption rate (SAR) among the samples. The high CDI performance of the CNb-oil series could be related to their well-developed hierarchical porosity, and functionalization of the structure with P-O-C units. Typically, the negative zeta potential of the CNb-oil series, possibly resulted from the P-O-C units, should play a substantial role in adsorbing the positively charged Na^+.

To further testify the above opinion, two control experiments were conducted (Figure S16). On one hand, the CDI system with both electrodes built by purely activated carbon was taken to absorb the salt with identical conditions to the ones shown above with applied voltage of 1.2 V. The SAC turns out to be ca. 20.5 $mg\,g^{-1}$, which is lower than the performance of CDI system above consisting of CNb-oil*1*-based electrode (for adsorbing Na^+) and activated carbon-based electrode (for adsorbing Cl^-). On the other hand, the performance of the CDI system with CNb-oil*1*-based electrode (for adsorbing Cl^-) and activated carbon-based electrode (for adsorbing Na^+) was also tested. Interestingly, the SAC further declines to 16.8 $mg\,g^{-1}$. These two experiments prove the substantial role of the surface charge of CNb-oil series on removing the salt.

Moreover, the adsorption-desorption cycling performance is another key factor determining the application prospect. Here the cycling testing was carried out in a two-electrode CDI system. As seen in Figure 5h, the capacity maintained at ca. 32 $mg\,g^{-1}$ after 30 cycles. This strongly demonstrates the superior capability of the CNb-oil series for CDI applications.

Conclusion

A general, metal-free method building on ketene chemistry has been developed to achieve low-cost bulk synthesis of carbon nanofibers. A classical reaction between P_2O_5 and plant oils results in alkylketenes which polymerize, and self-assemble to nanotube, which then condense at higher temperatures to form carbon nanofibers. Typically, the CNb-oil*1* possessed a high specific surface area (ca. 780 $m^2\,g^{-1}$) and hierarchical porosity with ultramicropores within the fiber structure (ca. 0.56 nm and ca. 0.84 nm). Due to leftovers of phosphorous in the structure, the carbon nanofibers are negatively charged in a broad pH range from 1 to 11, i.e., they are strongly acidic. Due to these advantages, CNb-oil*1* has high potential in many applications, and CDI was taken as an illustrative example here. Results show that the adsorption capacity of CNb-oil*1* can reach ca. 30 $mg\,g^{-1}$, which outperforms most of the reported pure carbon materials. Furthermore, the CNb-oil*1*-based electrode is very stable and was shown to last for at least 10000 adsorption-desorption cycles without performance loss.

Acknowledgements

Open Access funding enabled and organized by Projekt DEAL.

Conflict of Interest

The authors declare no conflict of interest.

Keywords: capacitive deionization · carbon nanofiber · metal free · phosphorus pentoxide · vegetable oil

[1] a) M. Antonietti, N. Lopez-Salas, A. Primo, *Adv. Mater.* **2019**, *31*, 1805719; b) M. Antonietti, M. Oschatz, *Adv. Mater.* **2018**, *30*, 1706836; c) N. Fechler, T. P. Fellinger, M. Antonietti, *Adv. Mater.* **2013**, *25*, 75 – 79; d) L. Klemeyer, H. Park, J. Huang, *ACS Mater. Lett.* **2021**, *3*, 511 – 515; e) X. Liu, M. Antonietti, *Adv. Mater.* **2013**, *25*, 6284 – 6290; f) X. Liu, N. Fechler, M. Antonietti, *Chem. Soc. Rev.* **2013**, *42*, 8237 – 8265; g) J. Zhu, K. Sakaushi, G. Clavel, M. Shalom, M. Antonietti, T. P. Fellinger, *J. Am. Chem. Soc.* **2015**, *137*, 5480 – 5485; h) Q. G. Wang, L. He, L. Y. Zhao, R. S. Liu, W. P. Zhang, A. H. Lu, *Adv. Funct. Mater.* **2020**, *30*, 1906117; i) C. Rosso, G. Filippini, A. Criado, M. Melchionna, P. Fornasiero, M. Prato, *ACS Nano* **2021**, *15*, 3621 – 3630; j) L. Zhang, M. Zhang, G. Liu, W. Jin, X. Li, *Adv. Funct. Mater.* **2021**, *31*, 2100110.

[2] a) A. Mehmood, G. Ali, B. Koyutürk, J. Pampel, K. Y. Chung, T.-P. Fellinger, *Energy Storage Mater.* **2020**, *28*, 101 – 111; b) L.-F. Chen, X.-D. Zhang, H.-W. Liang, M. Kong, Q.-F. Guan, P. Chen, Z.-Y. Wu, S.-H. Yu, *ACS Nano* **2012**, *6*, 7092 – 7102; c) J. Ge, L. A. Shi, Y. C. Wang, H. Y. Zhao, H. B. Yao, Y. B. Zhu, Y. Zhang, H. W. Zhu, H. A. Wu, S. H. Yu, *Nat. Nanotechnol.* **2017**, *12*, 434 – 440; d) X. Liu, M. Antonietti, *Carbon* **2014**, *69*, 460 – 466; e) S. Porada, F. Schipper, M. Aslan, M. Antonietti, V. Presser, T. P. Fellinger, *ChemSusChem* **2015**, *8*, 1867 – 1874; f) L. Zhang, Y. Wang, B. Peng, W. Yu, H. Wang, T. Wang, B. Deng, L. Chai, K. Zhang, J. Wang, *Green Chem.* **2014**, *16*, 3926; g) L. Zhang, S. Yang, Y. Lai, H. Liu, Y. Fan, C. Liu, H. Wang, L. Chai, *Appl. Catal. B* **2020**, *265*, 118556; h) W. Zhang, G. Cai, R. Wu, Z. He, H. B. Yao, H. L. Jiang, S. H. Yu, *Small* **2021**, *17*, 2004140; i) C. Ge, Y. Li, J.-J. Yin, Y. Liu, L. Wang, Y. Zhao, C. Chen, *NPG Asia Mater.* **2012**, *4*, e32.

[3] a) C. Zhao, S. Xiong, H. Li, Z. Li, C. Qi, H. Yang, L. Wang, Y. Zhao, T. Liu, *J. Power Sources* **2021**, *483*, 229188; b) K. Chiou, J. Huang, *Matter* **2020**, *3*, 302 – 319; c) T. Ouyang, K. Cheng, F. Yang, L. Zhou, K. Zhu, K. Ye, G. Wang, D. Cao, *J. Mater. Chem. A* **2017**, *5*, 14551 – 14561; d) V. Subramanian, H. Zhu, B. Wei, *Electrochem. Commun.* **2006**, *8*, 827 – 832; e) N. Xiao, Z. Ling, Y. Zhou, J. Qiu, *Carbon* **2013**, *61*, 386 – 394; f) K. Xie, K. Yuan, K. Zhang, C. Shen, W. Lv, X. Liu, J. G. Wang, B. Wei, *ACS Appl. Mater. Interfaces* **2017**, *9*, 4605 – 4613; g) W. Yang, L. Chen, X. Liu, X. Yue, C. Liu, J. Jia, *J. Mater. Chem. A* **2016**, *4*, 5834 – 5838; h) L. Shi, W. C. Li, X. Q. Zhang, A. H. Lu, *Adv. Mater. Interfaces* **2020**, *7*, 2000381; i) T. Liu, J. Serrano, J. Elliott, X. Yang, W. Cathcart, Z. Wang, Z. He, G. Liu, *Sci. Adv.* **2020**, *6*, eaaz0906.

[4] a) Y. Wen, H. Zhu, J. Hao, S. Lu, W. Zong, F. Lai, P. Ma, W. Dong, T. Liu, M. Du, *Appl. Catal. B* **2021**, *292*, 120144; b) H. W.

Liang, Q. F. Guan, L. F. Chen, Z. Zhu, W. J. Zhang, S. H. Yu, *Angew. Chem. Int. Ed.* **2012**, *51*, 5101 – 5105; *Angew. Chem.* **2012**, *124*, 5191 – 5195; c) Z. Y. Wu, C. Li, H. W. Liang, J. F. Chen, S. H. Yu, *Angew. Chem. Int. Ed.* **2013**, *52*, 2925 – 2929; *Angew. Chem.* **2013**, *125*, 2997 – 3001; d) J. Zhao, Y. Li, G. Wang, T. Wei, Z. Liu, K. Cheng, K. Ye, K. Zhu, D. Cao, Z. Fan, *J. Mater. Chem. A* **2017**, *5*, 23085 – 23093; e) J. Xiao, N. Xiao, C. Liu, H. Li, X. Pan, X. Zhang, J. Bai, Z. Guo, X. Ma, J. Qiu, *Small* **2020**, *16*, 2003827; f) J. C. Ruiz-Cornejo, D. Sebastián, M. J. Lázaro, *Rev. Chem. Eng.* **2020**, *36*, 493 – 511; g) L. Zou, M. Kitta, J. Hong, K. Suenaga, N. Tsumori, Z. Liu, Q. Xu, *Adv. Mater.* **2019**, *31*, 1900440.

[5] a) Y. Chang, M. Antonietti, T. P. Fellinger, *Angew. Chem. Int. Ed.* **2015**, *54*, 5507 – 5512; *Angew. Chem.* **2015**, *127*, 5598 – 5603; b) L. Li, Y. Li, Y. Ye, R. Guo, A. Wang, G. Zou, H. Hou, X. Ji, *ACS Nano* **2021**, *15*, 6872 – 6885; c) C.-T. Lin, T.-H. Chen, T.-S. Chin, C.-Y. Lee, H.-T. Chiu, *Carbon* **2008**, *46*, 741 – 746; d) L. Zhang, M. Wang, Y. Lai, X. Li, *J. Mater. Chem. A* **2018**, *6*, 4988 – 4996; e) C. Deeney, S. Wang, S. A. Belhout, A. Gowen, B. J. Rodriguez, G. Redmond, S. J. Quinn, *RSC Adv.* **2018**, *8*, 12907 – 12917; f) S. Chen, L. Qiu, H. M. Cheng, *Chem. Rev.* **2020**, *120*, 2811 – 2878; g) J. Y. Mao, F. Y. Lin, H. W. Chu, S. G. Harroun, J. Y. Lai, H. J. Lin, C. C. Huang, *J. Colloid Interface Sci.* **2019**, *552*, 583 – 596.

[6] J. Kalilainen, S. Nichenko, J. Krepel, *J. Nucl. Mater.* **2020**, *533*, 152134.

[7] X. Dupain, D. J. Costa, C. J. Schaverien, M. Makkee, J. A. Moulijn, *Appl. Catal. B* **2007**, *72*, 44 – 61.

[8] a) X. Dou, Y. Zheng, K. Uchiyama, J. M. Lin, *Chem. Commun.* **2016**, *52*, 14137 – 14140; b) Y. Fang, S. Guo, D. Li, C. Zhu, W. Ren, S. Dong, E. Wang, *ACS Nano* **2012**, *6*, 400 – 409; c) Y. Fang, E. Wang, *Nanoscale* **2013**, *5*, 1843 – 1848; d) X. Gong, Q. Hu, M. C. Paau, Y. Zhang, S. Shuang, C. Dong, M. M. Choi, *Nanoscale* **2014**, *6*, 8162 – 8170; e) W. Lei, Y.-P. Deng, G. Li, Z. P. Cano, X. Wang, D. Luo, Y. Liu, D. Wang, Z. Chen, *ACS Catal.* **2018**, *8*, 2464 – 2472; f) L. Liu, Z. Mi, Q. Hu, C. Li, X. Li, F. Feng, *Talanta* **2018**, *186*, 315 – 321; g) M. L. Liu, B. B. Chen, C. M. Li, C. Z. Huang, *Green Chem.* **2019**, *21*, 449 – 471; h) Y. Zhou, Z. Jia, L. Shi, Z. Wu, B. Jie, S. Zhao, L. Wei, A. Zhou, J. Zhu, X. Wang, Y. Fu, *Chem. Eng. J.* **2020**, *385*, 123858; i) P. Zuo, Z. Chen, F. Yu, J. Zhang, W. Zuo, Y. Gao, Q. Liu, *RSC Adv.* **2020**, *10*, 32919 – 32926; j) S. Y. Yu, J. Mahmood, H. J. Noh, J. M. Seo, S. M. Jung, S. H. Shin, Y. K. Im, I. Y. Jeon, J. B. Baek, *Angew. Chem. Int. Ed.* **2018**, *57*, 8438 – 8442; *Angew. Chem.* **2018**, *130*, 8574 – 8578.

[9] N. Sebbar, J. Appel, H. Bockhorn, *Combust. Sci. Technol.* **2016**, *188*, 745 – 758.

[10] H. Staudinger, *Ber. Dtsch. Chem. Ges.* **1905**, *38*, 1735 – 1739.

[11] G. A. Olah, E. Zadok, R. Edler, D. H. Adamson, W. Kasha, G. K. S. Prakash, *J. Am. Chem. Soc.* **1989**, *111*, 9123 – 9124.

[12] K. C. Khemani, F. Wudl, *J. Am. Chem. Soc.* **1989**, *111*, 9124 – 9125.

[13] M. A. Osman, J. Seibl, E. Pretsch, *Helv. Chim. Acta* **1977**, *60*, 3007 – 3011.

[14] W. B. Woodstock, US, **1951**.

[15] K. C. Kim, T.-U. Yoon, Y.-S. Bae, *Microporous Mesoporous Mater.* **2016**, *224*, 294 – 301.

[16] D. Iglesias, A. Giuliani, M. Melchionna, S. Marchesan, A. Criado, L. Nasi, M. Bevilacqua, C. Tavagnacco, F. Vizza, M. Prato, P. Fornasiero, *Chem* **2018**, *4*, 106 – 123.

[17] U. Biermann, W. Friedt, S. Lang, W. Lühs, G. Machmüller, J. O. Metzger, M. R. gen Klaas, H. J. Schafer, M. P. Schneider, *Angew. Chem. Int. Ed.* **2000**, *39*, 2206 – 2224; *Angew. Chem.* **2000**, *112*, 2292 – 2310.

Manuscript received: August 10, 2021
Accepted manuscript online: September 3, 2021
Version of record online: October 5, 2021

